

# Thermoelectric properties of half-Heusler ZrNiPb by using first principles calculations

San-Dong Guo

Department of Physics, School of Sciences, China University of Mining and Technology, Xuzhou 221116, Jiangsu, China

We investigate electronic structures and thermoelectric properties of recent synthetic half-Heusler ZrNiPb by using generalized gradient approximation (GGA) and GGA plus spin-orbit coupling (GGA+SOC). Calculated results show that ZrNiPb is an indirect-gap semiconductor. Within the constant scattering time approximation, semi-classic transport coefficients are performed through solving Boltzmann transport equations. It is found that the SOC has more obvious influence on power factor in p-type doping than in n-type doping, leading to a detrimental effect in p-type doping. These can be explained by considering the SOC influences on the valence bands and conduction bands near the Fermi level. The lattice thermal conductivity as a function of temperature is calculated, and the corresponding lattice thermal conductivity is  $14.5 \text{ Wm}^{-1}\text{K}^{-1}$  at room temperature. By comparing the experimental transport coefficients with calculated ones, the scattering time is attained for  $0.333 \times 10^{-14} \text{ s}$ . Finally, the thermoelectric figure of merit  $ZT$  can be attained, and the  $ZT$  value can be as high as 0.30 at high temperature by choosing appropriate doping level. It is possible to reduce lattice thermal conductivity by point defects and boundaries, and make half-Heusler ZrNiPb become potential candidate for efficient thermoelectricity.

PACS numbers: 72.15.Jf, 71.20.-b, 71.70.Ej, 79.10.-n

Keywords: Half-Heusler; Spin-orbit coupling; Power factor; Thermal conductivity

## INTRODUCTION

The performance of thermoelectric material can be characterized by the dimensionless thermoelectric figure of merit[1, 2],  $ZT = S^2\sigma T/(\kappa_e + \kappa_L)$ , where  $S$ ,  $\sigma$ ,  $T$ ,  $\kappa_e$  and  $\kappa_L$  are the Seebeck coefficient, electrical conductivity, absolute working temperature, the electronic and lattice thermal conductivities, respectively. Various thermoelectric materials have been identified, such as relatively low temperature operation Bismuth-tellurium systems[3, 4], high temperature operation silicon-germanium alloys[5, 6], moderate temperature operation lead chalcogenides[7, 8]. Heusler compounds can be applied to spintronics, superconductors, topological insulators and thermoelectrics[9]. Due to being environmentally friendly, mechanically and thermally robust, 18-valence electron half-Heusler has been widely investigated for thermoelectric application[10–13]. Many theoretical reports on thermoelectric properties of half-Heusler focus on electronic part[14–20, 25]. Recently, the lattice thermal conductivities of half-Heusler alloy TiNi<sub>3</sub>Sn and ZrCoSb by first principles calculations are attained, and the calculated lattice thermal conductivities are close to the experimental values[21, 22].

In ref.[23], by using first principles calculations, 54 of the 400 unreported 18-valence electron half-Heuslers should be stable, and 15 have been grown, whose X-ray experimental results agree with the predicted crystal structures. ZrNiPb is synthesized as a single phase, and the room temperature power factor is as high as  $5.2 \mu\text{Wcm}^{-1}\text{K}^{-2}$ . However, the thermal conductivity of ZrNiPb hasn't been measured by the related experiments. Here, the electronic structures and thermoelectric properties of half-Heusler ZrNiPb are studied by the first principles calculations and Boltzmann transport

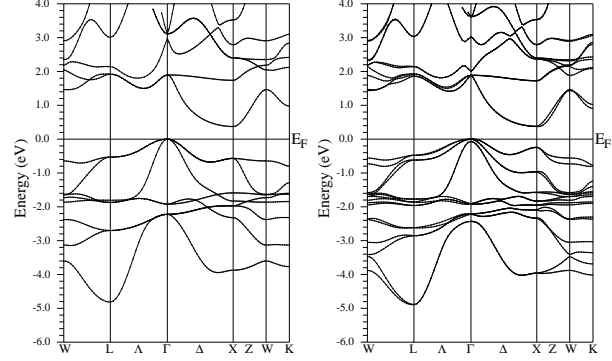


FIG. 1. The energy band structures of ZrNiPb by using GGA (Left) and GGA+SOC (Right).

equations within the constant scattering time approximation. The SOC has been proved to be very important for power factor calculations of many thermoelectric materials[20, 24, 26], so the SOC effect is considered in our calculations. Calculated results show SOC has larger effects on power factor in p-type doping than in n-type doping, and has a reduced influence for p-type. In this work, the electronic part of thermoelectric properties of half-Heusler ZrNiPb is not only calculated, but also the lattice lattice thermal conductivity is attained. The calculated room temperature lattice thermal conductivity is  $14.5 \text{ Wm}^{-1}\text{K}^{-1}$ . Although calculating scattering time is difficult, it can be attained by the comparison between experimental and calculated transport coefficients. Finally, the dimensionless thermoelectric figure of merit  $ZT$  is calculated, and can be up to 0.3 at high temperature by the optimized doping.

The rest of the paper is organized as follows. In the next section, we shall give our computational details. In

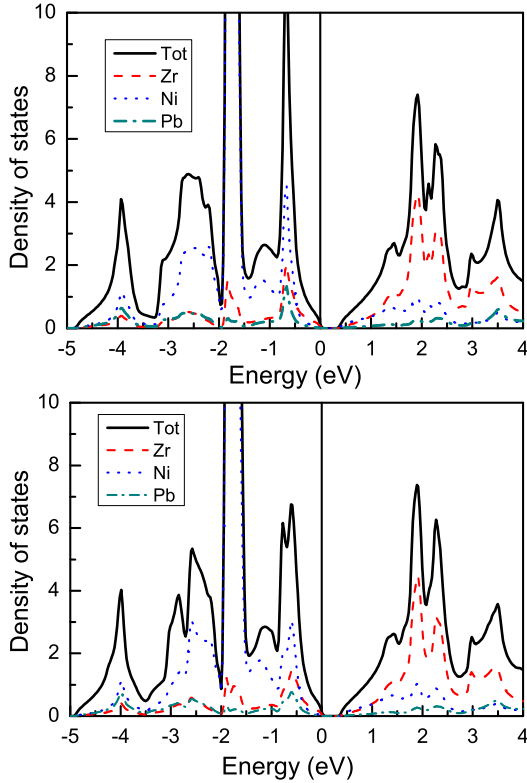


FIG. 2. (Color online) The total and partial densities of states of ZrNiPb by using GGA (Top panel) and GGA+SOC (Bottom panel).

the third section, we shall present our main calculated results and analysis. Finally, we shall give our conclusion in the fourth section.

### COMPUTATIONAL DETAIL

We use a full-potential linearized augmented-plane-waves method within the density functional theory (DFT) [27], as implemented in the package WIEN2k [28]. We use GGA [29] to do our main DFT calculations. The full relativistic effects are calculated with the Dirac equations for core states, and the scalar relativistic approximation is used for valence states [30–32]. The SOC was included self-consistently by solving the radial Dirac equation for the core electrons and evaluated by the second-variation method[33]. We use 10000 k-points in the first Brillouin zone for the self-consistent calculation. We make harmonic expansion up to  $l_{\max} = 10$  in each of the atomic spheres, and set  $R_{\text{mt}} * k_{\max} = 8$ . The self-consistent calculations are considered to be converged when the integration of the absolute charge-density difference between the input and output electron density is less than  $0.0001|e|$  per formula unit, where  $e$  is the electron charge. Transport calculations are performed through solving Boltzmann transport

equations within the constant scattering time approximation as implemented in BoltzTrap[34], which has been applied successfully to several materials[35–37]. To obtain accurate transport coefficients, we use 200000 k-points in the first Brillouin zone for the energy band calculation. The lattice thermal conductivities are calculated by using Phono3py+VASP codes[38–41]. For the third-order force constants,  $2 \times 2 \times 2$  supercells are built, and reciprocal spaces of the supercells are sampled by  $2 \times 2 \times 2$  meshes. To compute lattice thermal conductivities, the reciprocal spaces of the primitive cells are sampled using the  $20 \times 20 \times 20$  meshes.

### MAIN CALCULATED RESULTS AND ANALYSIS

The 18-valence electron half-Heusler ZrNiPb possesses, forming a MgAgAs type of structure, space group  $F\bar{4}3m$ , where Zr, Ni, and Pb atoms occupy Wyckoff positions 4a (0, 0, 0), 4c (1/4, 1/4, 1/4) and 4b (1/2, 1/2, 1/2) positions, respectively. The optimized lattice constants  $a=6.27$  Å is used to do our DFT calculations, and present energy band structures and density of states (DOS) by using GGA and GGA+SOC in Figure 1 and Figure 2. ZrNiPb is a indirect-gap semiconductor, with the conduction band minimum (CBM) at high symmetry point X and valence band maximum (VBM) at the  $\Gamma$  point, and the energy band gap value is about 0.37 eV by using both GGA and GGA+SOC. The DOS's show that the strong hybridization of d states of Zr and Ni atoms produces the energy band gap. The bottom of the conduction bands are constructed mostly by Zr-d and Ni-d states, while the valence bands near the Fermi level are dominated by the Zr-d state hybridized with the Ni-d and Pb-p states. The SOC can remove the band degeneracy. It is clearly seen that SOC leads to a remarkable spin-orbital splitting value of 0.73 eV at high symmetry X point of valence bands near the Fermi level, and 0.07 eV at  $\Gamma$  point. The SOC has weaker effect on the conduction bands near the Fermi level than on the valence bands. Compared to half-Heusler ANiB (A=Ti, Hf, Sc, Y; B=Sn, Sb, Bi)[20], a major difference is that the energy between VBM and the extremum of valence at X point is more close, which leads to different SOC effects on Seebeck coefficient.

Here, the band structures are supposed to be independent of the temperature and doping, and the semi-classic transport coefficients as a function of doping level are calculated within constant scattering time approximation Boltzmann theory. Figure 3 shows the Seebeck coefficient S, electrical conductivity with respect to scattering time  $\sigma/\tau$  and power factor with respect to scattering time  $S^2\sigma/\tau$  as a function of doping levels at the temperature of 300 K by using GGA and GGA+SOC. The negative doping levels, being related with conduction bands, imply the n-type doping with the negative

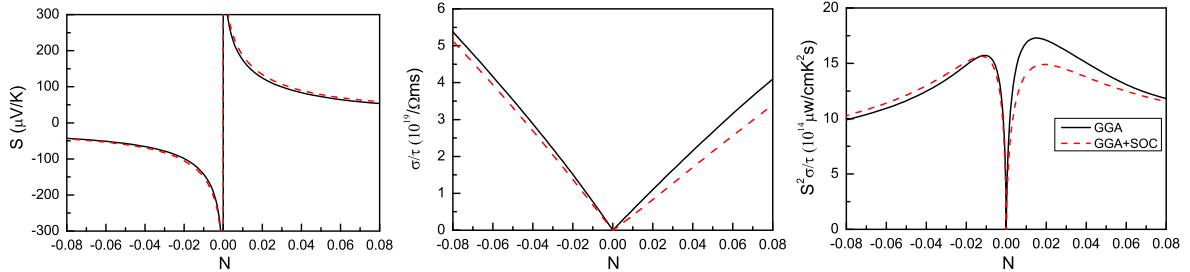


FIG. 3. (Color online) At temperature of 300 K, transport coefficients as a function of doping levels (electrons [minus value] or holes [positive value] per unit cell): Seebeck coefficient  $S$  (Left), electrical conductivity with respect to scattering time  $\sigma/\tau$ , (Middle) and power factor with respect to scattering time  $S^2\sigma/\tau$  (Right) calculated with GGA (Solid line) and GGA+SOC (Dotted line).

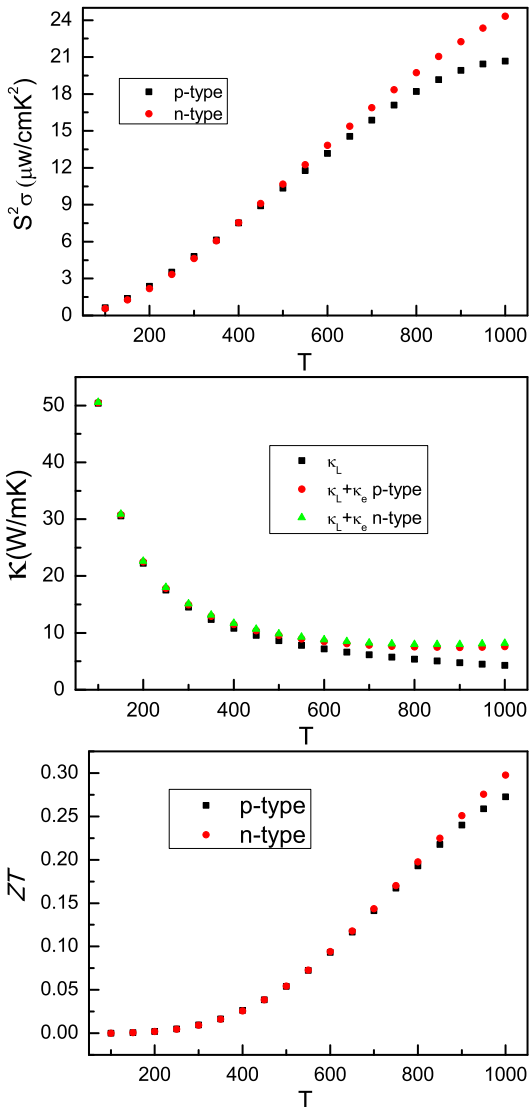


FIG. 4. (Color online) The power factor  $S^2\sigma$ , thermal conductivity  $\kappa$  (electronic  $\kappa_e$  and lattice  $\kappa_L$  thermal conductivities) and  $ZT$  as a function of temperature with the doping concentration of  $5 \times 10^{20} \text{ cm}^{-3}$  for p-type and n-type, and the scattering time  $\tau$  is  $0.333 \times 10^{-14} \text{ s}$ .

Seebeck coefficient, and the positive doping levels, being connected with valence bands, mean p-type doping with the positive Seebeck coefficient.

In narrow-gap semiconductors, the large slope of DOS near the energy gap may give rise to a large Seebeck coefficient[25]. Calculated results show that the slope of DOS by using GGA+SOC near the energy band gap is larger than that by using GGA for both valence and conduction bands. Calculated results show, in both p-type and n-type doping, SOC has an enhanced influence on the Seebeck coefficient  $S$  (absolute value). This is different from half-Heusler ANiB ( $A=\text{Ti, Hf, Sc, Y}$ ;  $B=\text{Sn, Sb, Bi}$ )[20], which is due to closer valence extremum between  $\Gamma$  and  $X$  points(Band degeneracy, namely band convergence, can enhance Seebeck coefficient[24, 42], and here is SOC driven degeneracy.). However, the SOC has a detrimental influence on the  $\sigma/\tau$  for both p-type and n-type doping, which can be explained by that SOC leads to more localized bands. When SOC isn't considered, the best power factor in p-type doping is larger than that in n-type. However, including SOC, the best n-type power factor is larger than the best p-type one in considered doping range. Similar SOC effects on best power factor can be found in  $\text{Mg}_2\text{Sn}$ [24], which agrees well with experimental results. In n-type doping, SOC can reduce the power factor in low doping levels, but can also enhance one in high doping levels. In p-type doping, SOC has more obvious effect on power factor, leading to a detrimental influence in the considered doping levels. The maximum power factor (MPF) by using GGA+SOC in p-type doping is about 13.8% smaller than that with GGA. Therefore, it is necessary to consider SOC in the theoretical prediction of thermoelectric properties of  $\text{ZrNiPb}$ .

Calculating  $\tau$  from the first principles is challenging, but it can be attained by comparing the related experimental results. At room temperature, the measured electron conductivity and Seebeck coefficient of  $\text{ZrNiPb}$  are  $220.1 \Omega^{-1}\text{cm}^{-1}$  and  $-153.9 \mu\text{VK}^{-1}$ , respectively, which gives a power factor  $5.2 \mu\text{Wcm}^{-1}\text{K}^{-2}$ [23]. By comparing measured and calculated Seebeck coefficient, the doping level is determined to be  $-0.0097$ , and the  $\tau$  is attained

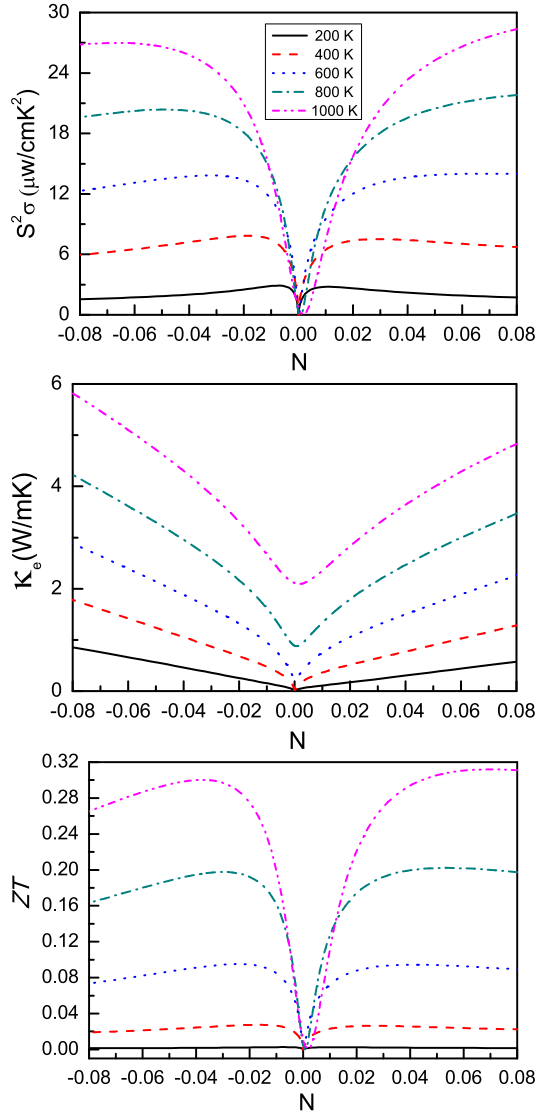


FIG. 5. (Color online) The power factor, electronic thermal conductivity and  $ZT$  as a function of doping levels with temperature being 200, 400, 600, 800 and 1000 (unit: K), and the scattering time  $\tau$  is  $0.333 \times 10^{-14}$  s.

for  $0.333 \times 10^{-14}$  s by making a comparison between experimental and theoretical electron conductivities. The power factor  $S^2\sigma$  with the doping level  $-0.0097$  is calculated by using  $\tau=0.333 \times 10^{-14}$  s, and the attained value is  $5.16 \mu\text{Wcm}^{-1}\text{K}^{-2}$ , being in agreement with experimental value  $5.2 \mu\text{Wcm}^{-1}\text{K}^{-2}$ , which confirms the reliability of our calculated results.

Here, we assume that the relaxation time  $\tau$  is temperature and doping level independent. The power factor  $S^2\sigma$ , lattice thermal conductivity  $\kappa_L$ , total thermal conductivity  $\kappa=\kappa_e+\kappa_L$  and  $ZT$  as a function of temperature with the doping concentration of  $5 \times 10^{20}\text{cm}^{-3}$  (The doping concentration equals  $1.625 \times 10^{22}\text{cm}^{-3} \times$  doping level.) for both p-type and n-type are shown in Figure 4.

In low temperature region, there is little difference between n-type power factor and p-type one. At  $T=1000$  K, the power factor is as high as  $24.3 \mu\text{Wcm}^{-1}\text{K}^{-2}$  for n-type doping, and  $20.7 \mu\text{Wcm}^{-1}\text{K}^{-2}$  for p-type doping. The lattice thermal conductivity can be assumed to be independent of doping levels, and typically goes as  $1/T$ . At room temperature, the corresponding lattice thermal conductivity is  $14.5 \text{Wm}^{-1}\text{K}^{-1}$ , which is among the reported room temperature lattice thermal conductivity of half-Heuslers ( $6.7\text{--}20 \text{Wm}^{-1}\text{K}^{-1}$ )[12]. At low  $T$ , the total thermal conductivity  $\kappa$  is dominated by the  $\kappa_L$ , but lattice thermal conductivity  $\kappa_L$  and electronic thermal conductivity  $\kappa_e$  have the same order of magnitude at high temperature region. At  $T=1000$  K, the  $ZT$  is as high as 0.30 for n-type doping, and 0.27 for p-type doping. The high lattice thermal conductivity leads to relatively small  $ZT$  value. Finally, the power factor  $S^2\sigma$ , electronic thermal conductivity  $\kappa_e$  and  $ZT$  as a function of doping levels with temperature being 200, 400, 600, 800 and 1000 (unit: K) are plotted in Figure 5. It is found that electronic thermal conductivity increases with the increasing temperature. Calculated results show that the higher  $ZT$  can be attained in high doping levels at high temperature region.

## DISCUSSIONS AND CONCLUSION

For thermoelectric device applications, although half-Heusler  $\text{ZrNiPb}$  has high power factor, high lattice thermal conductivity ( $14.5 \text{Wm}^{-1}\text{K}^{-1}$  at room temperature) is a major disadvantage. It has been shown that lattice thermal conductivity can be reduced by point defects and boundaries. The binary or ternary alloying of Hf, Zr and Ti in M site of n-type  $\text{MNiSn}$  and p-type  $\text{MCoSb}$  ( $\text{M}=\text{Hf}$ ,  $\text{Zr}$  and  $\text{Ti}$ ) can reduce the thermal conductivity compared with a single element  $\text{MNiSn}$ [43–46]. The smaller grain size can effectively suppress the thermal conductivity. The thermal conductivity of  $\text{TiNiSn}_{1-x}\text{Sb}_x$  is about  $3.7 \text{Wm}^{-1}\text{K}^{-1}$  with an average grain size of 50 nm[47], and the room temperature thermal conductivity is also  $3.7 \text{Wm}^{-1}\text{K}^{-1}$  at grain sizes below 200 nm for p-type  $\text{Hf}_{0.5}\text{Zr}_{0.5}\text{CoSn}_{0.8}\text{Sb}_{0.2}$ [48]. Therefore, experimentally, it is possible to reduce the thermal conductivity of  $\text{ZrNiPb}$  by point defects (doping  $\text{ZrNiPb}$  with Hf) and boundaries (reducing grain size).

In summary, we investigate thermoelectric properties of  $\text{ZrNiPb}$  based mainly on the reliable first-principle calculations, including not only electronic but also lattice part. The electronic part, including power factor and electronic thermal conductivity, is calculated by using GGA+SOC, while lattice thermal conductivity is performed with GGA. It is found that SOC is very important for p-type power factor calculations, and has a obvious detrimental influence. Calculated results show that  $\text{ZrNiPb}$  has high power factor, but high thermal conduction.

tivity is a fatal disadvantage to gain high  $ZT$  value. So, reducing the lattice thermal conductivity is very key to attain better thermoelectric performance. The present work is useful for further improving thermoelectric performance of half-Heusler ZrNiPb.

This work is supported by the Fundamental Research Funds for the Central Universities (2015XKMS073). We are grateful to the Advanced Analysis and Computation Center of CUMT for the award of CPU hours to accomplish this work.

---

[1] Y. Pei, X. Shi, A. LaLonde, H. Wang, L. Chen, G. J. Snyder, *Nature* **473**, 66 (2011).

[2] A. D. LaLonde, Y. Pei, H. Wang and G. J. Snyder, *Mater. Today* **14**, 526 (2011).

[3] W. S. Liu, Q. Y. Zhang, Y. C. Lan, S. Chen, X. Yan, Q. Zhang, H. Wang, D. Z. Wang, G. Chen and Z. F. Ren, *Adv. Energy Mater.* **1**, 577 (2011).

[4] D. K. Ko, Y. J. Kang and C. B. Murray, *Nano Lett.* **11**, 2841 (2011).

[5] M. Zebarjadi, et al., *Nano Lett.* **11**, 2225 (2011).

[6] B. Yu, et al., *Nano Lett.* **12**, 2077 (2012).

[7] Y. Z. Pei, X. Y. Shi, A. Lalonde et al, *Nature* **473**, 66 (2011).

[8] J. Q. He, J. R. Sootsman, S. N. Girard et al., *J. Am. Chem. Soc.* **132**, 8669 (2010).

[9] T. Graf, C. Felser and Stuart S.P. Parkin, *Prog. Solid State Ch.* **39**, 1 (2011).

[10] J. R. Sootsman, *Angew. Chem.* **48**, 8616 (2009).

[11] M. Schwall and B. Balke, *Appl. Phys. Lett.* **98**, 042106 (2011).

[12] S. Chen and Z. F. Ren, *Mater. Today* **16**, 387 (2013).

[13] J. Yang, et al. *Adv. Funct. Mater.* **18**, 2880 (2008).

[14] J. Yang, H. M. Li, T. Wu, W. Q. Zhang, L. D. Chen and J. H. Yang, *Adv. Funct. Mater.* **18**, 2880 (2008).

[15] S. Ouardi, G. H. Fecher, B. Balke, X. Kozina, G. Stryganyuk and C. Felser, *Phys. Rev. B* **82**, 085108 (2010).

[16] M. S. Lee, Ferdinand P. Poudeu and S. D. Mahanti, *Phys. Rev. B* **83**, 159907 (2011).

[17] D. F. Zou, S. H. Xie, Y. Y. Liu, J. G. Lin and J. Y. Li, *J. Appl. Phys.* **113**, 193705 (2013).

[18] M. K. Yadav, B. Sanyal, *J. Alloy. Compd.* **622**, 388 (2015).

[19] G. Q. Ding, G. Y. Gao and K. L. Yao, *J. Phys. D: Appl. Phys.* **47**, 385305 (2014).

[20] S. D. Guo, *J. Alloy. Compd.* **663**, 128 (2016).

[21] G. Q. Ding, G. Y. Gao and K. L. Yao, *J. Phys. D: Appl. Phys.* **48**, 235302 (2015).

[22] J. Shiomi, K. Esfarjani, and G. Chen, *Phys. Rev. B* **84**, 104302 (2011).

[23] R. Gautier, X. W. Zhang et al, *Nat. Chem.* **7**, 308 (2015).

[24] S. D. Guo and J. L. Wang, *RSC Adv.* in press (DOI: 10.1039/C6RA01376G).

[25] M. ONUOE, F. ISHII and T. OGUCHI, *J. Phys. Soc. Jpn.* **77**, 054706 (2008).

[26] K. Kutorasinski, B. Wiendlocha, J. Tobola and S. Kaprzyk, *Phys. Rev. B* **89**, 115205 (2014).

[27] P. Hohenberg and W. Kohn, *Phys. Rev.* **136**, B864 (1964); W. Kohn and L. J. Sham, *Phys. Rev.* **140**, A1133 (1965).

[28] P. Blaha, K. Schwarz, G. K. H. Madsen, D. Kvasnicka and J. Luitz, WIEN2k, an Augmented Plane Wave + Local Orbitals Program for Calculating Crystal Properties (Karlheinz Schwarz Technische Universität Wien, Austria) 2001, ISBN 3-9501031-1-2

[29] J. P. Perdew, K. Burke and M. Ernzerhof, *Phys. Rev. Lett.* **77**, 3865 (1996).

[30] A. H. MacDonald, W. E. Pickett and D. D. Koelling, *J. Phys. C* **13**, 2675 (1980).

[31] D. J. Singh and L. Nordstrom, *Plane Waves, Pseudopotentials and the LAPW Method*, 2nd Edition (Springer, New York, 2006).

[32] J. Kunes, P. Novak, R. Schmid, P. Blaha and K. Schwarz, *Phys. Rev. B* **64**, 153102 (2001).

[33] D. D. Koelling, B. N. Harmon, *J. Phys. C Solid State Phys.* **10**, 3107 (1977).

[34] G. K. H. Madsen and D. J. Singh, *Comput. Phys. Commun.* **175**, 67 (2006).

[35] B. L. Huang and M. Kaviany, *Phys. Rev. B* **77**, 125209 (2008).

[36] L. Q. Xu, Y. P. Zheng and J. C. Zheng, *Phys. Rev. B* **82**, 195102 (2010).

[37] J. J. Pulikkotil, D. J. Singh, S. Auluck, M. Saravanan, D. K. Misra, A. Dhar and R. C. Budhani, *Phys. Rev. B* **86**, 155204 (2012).

[38] G. Kresse, *J. Non-Cryst. Solids* **193**, 222 (1995).

[39] G. Kresse and J. Furthmüller, *Comput. Mater. Sci.* **6**, 15 (1996).

[40] G. Kresse and D. Joubert, *Phys. Rev. B* **59**, 1758 (1999).

[41] A. Togo, L. Chaput and I. Tanaka, *Phys. Rev. B* **91**, 094306 (2015).

[42] W. Liu, X. J. Tan, K. Yin, H. J. Liu, X. F. Tang, J. Shi, Q. J. Zhang, and C. Uher, *Phys. Rev. Lett.* **108**, 166601 (2012).

[43] S. Bhattacharya, M. J. Skove, M. Russell, T. M. Tritt, Y. Xia, V. Ponnambalam, S. J. Poon and N. Thadhani *Phys. Rev. B* **77**, 184203 (2008).

[44] V. Ponnambalam, P. N. Alboni, J. Edwards, T. M. Tritt, S. R. Culp and S. J. Poon, *J. Appl. Phys.* **103**, 063716 (2008).

[45] P. F. Qiu, X. Y. Huang, X. H. Chen and L. D. Chen, *J. Appl. Phys.* **106**, 103703 (2009).

[46] N. Shutoh and S. Sakurada, *J. Alloy. Compd.* **389**, 204 (2005).

[47] S. Bhattacharya, T. M. Tritt, Y. Xia, V. Ponnambalam, S. J. Poon and N. Thadhani, *Appl. Phys. Lett.* **81**, 43 (2002).

[48] X. Yan, G. Joshi, et al. *Nano Lett.* **11**, 556 (2011).